Article

Experimental and Numerical Study on Dynamics of Two Footbridges with Different Shapes of Girders

Anna Banas * and **Robert Jankowski**

Faculty of Civil and Environmental Engineering, Gdansk University of Technology, 80-233 Gdansk, Poland; jankowr@pg.edu.pl

* Correspondence: anna.banas@pg.edu.pl

Abstract: The paper presents the experimental and numerical results of the dynamic system identification and verification of the behavior of two footbridges in Poland. The experimental part of the study involved vibration testing under different scenarios of human-induced load, impulse load, and excitations induced by vibration exciter. Based on the results obtained, the identification of dynamic parameters of the footbridges was performed using the peak-picking method. With the impulse load applied to both structures, determination of their natural vibration frequencies was possible. Then, based on the design drawings, detailed finite element method (FEM) models were developed, and the numerical analyses were carried out. The comparison between experimental and numerical results obtained from the modal analysis showed a good agreement. The results also indicated that both structures under investigation have the first natural bending frequency of the deck in the range of human-induced excitation. Therefore, the risk of excessive structural vibrations caused by pedestrian loading was then analysed for both structures. The vibration comfort criteria for both footbridges were checked according to Sétra guidelines. In the case of the first footbridge, the results showed that the comfort criteria are fulfilled, regardless of the type of load. For the second footbridge, it was emphasized that the structure meets the assumptions of the guidelines for vibration severability in normal use; nevertheless, it is susceptible to excitations induced by synchronized users, even in the case of a small group of pedestrians.

Keywords: footbridges; dynamic loads; experimental study; numerical analysis; human-induced vibrations

1. Introduction

Dynamic loads are among the most dangerous and unpredicted threats that can be observed in the case of civil engineering structures [1–3]. Structural vibrations induced by wind, earthquakes, mining tremors, or behavior of people (human-induced vibrations) may lead to damages of structures or serious effects on the health of the users (e.g., [4–8]). Relatively light and slender footbridges are among different types of structures which are susceptible to dangerous vibrations under dynamic excitations [9]. The problem especially concerns new structures designed using new construction solutions and materials. This is due to the fact that the vibration frequencies of the modern footbridges are often close to the frequencies which are induced by pedestrians [10–18]. The well-known examples of footbridges that experienced excessive vibrations during exploitation are the Millenium bridge in London [10–12], the Solferino bridge in Paris [13,14], and the Mape Valley Great Suspension Bridge [19]. Fortunately, in most of the cases, vibrations were not related to the ultimate limit state but only to the comfort of the users. For this reason, it was necessary to introduce norms and guidelines to the designing process that will allow estimating the vibration comfort of the footbridges [20–23]. The French Sétra guidelines [24] and the European guidelines "Human-induced vibration of steel

structures" (HiVoss) [25] are the examples of the most commonly used guidelines related to the criterion of vibrational comfort at footbridges.

In order to provide appropriate comfort conditions, many footbridges are currently equipped with additional damping devices. Among them, the Pedro e Ines footbridge in Coimbra [15,16], Changi Mezzanine Bridge [26,27], the Footbridge of VW Autostadt in Wolfsburg [28], and tensegrity Kurilpa footbridge [29] can be mentioned. The commonly used devices suppressing excessive vibrations are tuned mass dampers, liquid dampers [19], viscous dampers [30], and active tendons [31].

In order to assess the behavior of the structure, and the risk of occurrence of excessive vibrations, whether at the design or the operation stage, knowledge of its basic dynamic characteristics is mandatory. These modal quantities are natural frequencies, damping ratios, and mode shapes. They can be determined by experimental tests or estimated through numerical analysis.

The experimental tests can be carried out on existing structures. The results obtained during the field tests give the objective knowledge of the dynamic structural behavior. A description of the basic steps to identify dynamic parameters of the structure could be found in [32]. They included the creation of a priori models, vibration testing, post-processing of received data, validation and calibration, and also the utilization of a numerical model in some cases [33]. During the experimental study, two basic methods could be distinguished to find out the modal parameters. The first of them was based on the correlation between input data, excitations; and output data, responses of the structure [34–36]. The second one, called the operational modal analysis (OMA) or ambient modal analysis, was based solely on output data [37–39]. There are many methods for the identification of dynamic parameters of structures. The most commonly used are the peak—picking method [39], frequency domain decomposition [40], the random decrement technique [41], frequency—domain direct parameter identification method [42], stochastic subspace identification methods [43], and eigensystem realisation algorithm [44]. A good review of the literature on modal identification techniques can be found in [39,45,46]. Furthermore, in the literature [38,39,47–49], a comparison of the dynamic parameters identification carried out by various methods could be found.

The modal parameters obtained from experimental tests could also be used further in updating [50–58], structural health monitoring (SHM) [59–62], non-destructive diagnostics [63–65], and others.

The second approach intended to estimate the dynamic properties of structures is to conduct numerical analysis. The use of the numerical models of real structures to perform modal analysis had many advantages. It allowed us to predict (i.e., at the design stage) the expected levels of acceleration caused by the human-induced load. Thus, if the comfort level was exceeded, the modification of the structure was possible. However, there is one disadvantage. The creation of a numerical model that sufficiently reliably describes the dynamic properties of a real structure is a very complex issue [50]. It is due to a large number of unknowns at this stage, including estimation of the damping ratio, appropriate boundary conditions, modeling of joints, material properties, and the influence of non-structural elements on dynamic parameters of the structure [66]. Therefore, the best practice is the development of the numerical model, followed by dynamic field tests to confirm the assumptions. Another important issue is how to model the human-induced load. There are many models which can be used, but it should be remembered that walking behavior is an individual feature. It also depends mainly on synchronization with the structure and with other pedestrians. The human–structure interaction (HSI) phenomena were widely investigated in the literature [67–72]. Therefore, it is not easy to develop one universal model describing human-induced load [73].

The paper presents an experimental and numerical investigation focused on two examples of footbridges in Poland. Both footbridges had reinforced concrete decks and steel girders. One of the structures was an example of a typical arch bridge, while the second was characterized by the unusual shape of the steel girder. It was decided to compare both structures and examine the influence of the unusual shape of the girder on the dynamic parameters. For both structures, the detailed experimental tests and numerical analyses were conducted. The field tests were carried out under different sets of

pedestrian crowd loads. Various human-induced load scenarios allowed us to draw conclusions about the risk of excessive vibrations during exploitation. Hence, based on the obtained acceleration time histories, it was possible to assess the level of comfort. The footbridges were also tested under an impulse load and excitations induced by a light vibration exciter, so as to identify dynamic parameters, such as natural frequencies, mode shapes, and damping ratios. The dynamic parameters of both footbridges considered in numerical analyses were verified by comparing them with the results from the field tests.

The article is arranged as follows. In Section 2, the footbridges and created numerical FEM models are described. The theoretical basics of the dynamic and modal analysis are presented altogether with data processing and mode shapes and frequencies validation criteria. A field test conducted on the designed footbridges, consisting of acceleration measurements, is also described in this section. Subsequently, the results from the numerical analysis and the field test are compared and discussed in Section 3. In this section, the comfort criteria for both footbridges based on the accelerations obtained in field tests were also assessed. Finally, conclusions were presented in Section 4.

2. Materials and Methods

2.1. Footbridge Descriptions

2.1.1. Example 1

The first structure under investigation is the arch footbridge located above an expressway S8 in Poland (Figure 1). It was built in 2013 as a connection between two vehicle service places. It has a length of 50.0 m, a total width of 4.5 m, and a height of about 7.5 m (Figure 2). The superstructure consists of two parallel steel arch beams, a reinforced concrete deck, and fourteen vertical hangers. The cross-section of the arch beam is made of a circular pipe with diameter of 660.4 mm and thickness of 20 mm. The arches are joined by five pipe bracings with diameter of 323.9 mm and thickness of 10 mm. Steel rods with a diameter of 56 mm are used as hangers. The cross-section of the deck consists of two beams of 0.60 m height, connected with a slab with thickness of about 0.20 m. A pair of elastomeric bearings have been installed at each abutment to support the superstructure. Reinforced concrete abutments are founded on large diameter piles.

Figure 1. Side and front view of the arch footbridge above expressway S8.
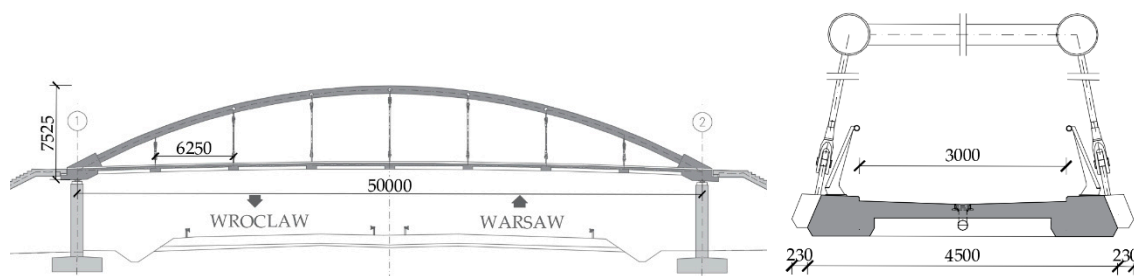

Figure 2. General structural arrangement and typical cross-section of the arch footbridge above expressway S8 (dimensions in mm).

2.1.2. Example 2

The second structure is a footbridge located above the University Route in Bydgoszcz, Poland (Figure 3). The construction of the University Route was planned from the 1970s and was finally built in 2013 connecting the Lower City's Terrace with the Upper City's Terrace. The footbridge has a length of 34.40 m, a width of 4.5 m, and height above girder supports of more than 20 m. The span consists of a reinforced deck, steel girders, and 14 hangers. Steel girders have an unusual shape similar to a triangle, and their cross-section resembles a tear with height of 720 mm, width of 900 mm, and thickness of 20 mm. The deck has been constructed as a reinforced concrete slab with a variable thickness from 0.18 m in the longitudinal axis of the structure to 0.45 m in the external zones. The hangers are made of closed rods with a diameter of 0.06 m. The arrangement of the girders has been founded on three support blocks set on piles. The platform is based on elastomeric bearings on reinforced concrete abutments, which sit on footing types of foundations. The main geometries and dimensions of the structure are shown in Figure 4.

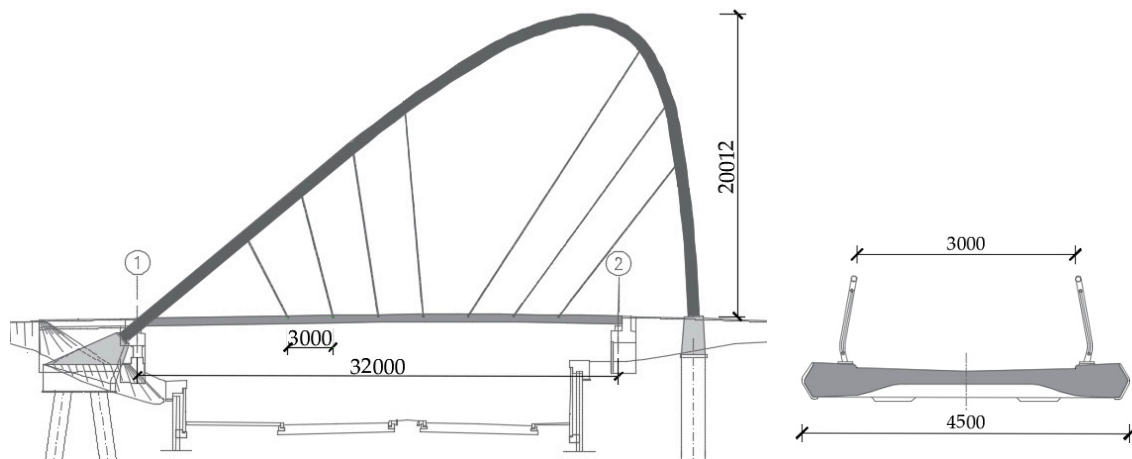**Figure 3.** Side and front view of the footbridge above the University Route in Bydgoszcz.

Figure 4. General structural arrangement and typical cross-section of the footbridge above the University Route in Bydgoszcz (dimensions in mm).

2.2. Vibration Testing

Both of the analyzed footbridges underwent static and dynamic field tests. During the static tests, displacements of the deck, settlements of the supports and forces in hangers were measured. The dynamic tests included measurements of the vertical displacements of the deck, an increase of strains in the hangers and accelerations of the platform and the arch or steel girder.

Three-axial, micro-electro-mechanical capacitive accelerometers (MEMS) of the LIS344ALH type manufactured by STMicroelectronics (Figure 5a) were used to measure the structure vibration response [74,75]. They consist of a seismic mass suspended on a spring, for which length depends on the level of acceleration (see also [76]). A change in the length of the spring causes a change in the capacitance of the capacitor connected. In consequence, the electronic system contained in the accelerometer generates a voltage proportional to the capacitor's capacity. The LIS344ALH has a full-scale of ±2 g/±6 g, and the device is capable of measuring accelerations over a maximum bandwidth of 1.8 kHz for all axes. The sensor has small dimensions of $4 \times 4 \times 1.5$ mm and a weight of 0.040 g. The operating temperature is between $-40\sim85$ °C. The measurement data were recorded using the QUANTUM HBM 840a 8-channel measurement amplifier (Figure 5d). A standard laptop was connected to the measuring station and it was used for the data processing, visualization, and storage of the measurement results. During the tests, accelerometers were placed in such a way that one axis was perpendicular to the axis of the deck, the second axis was vertical, and the third one was longitudinal. In each case, the accelerometers were rigidly connected to the platform of structure, either with concrete screws (Figure 5b) or with strong neodymium magnets and additionally compressed with the clamp elements of the hangers anchor (Figure 5c). The sampling rate was set to 600 Hz.
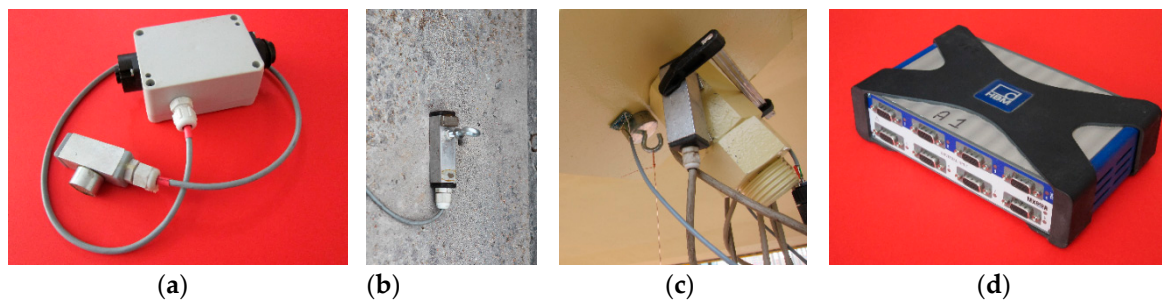

(**a**) (**b**) (**c**) (**d**)

Figure 5. (**a**) Tri-axial MEMS accelerometer in a case; (**b**) Example of attaching the accelerometer on the concrete deck of footbridge; (**c**) Example of attaching the accelerometer on the elements of the hangers anchor of footbridge; (**d**) QUANTUM HBM 840a 8-channel measurement amplifier.

As the main excitation of the footbridges is related to the movement of pedestrians, dynamic measurements were taken during the following tests: free and synchronized march, free and synchronized run and jumping (Figure 6). Depending on the test, 6, 9, and 12 pedestrian groups were used as a dynamic load. This allowed studying the influence of the increasing number of pedestrians on the values of received accelerations. In all tests related to walking or free running, each pedestrian was moving at their own pace. However, the synchronous excitations were harmonized using a metronome. In the case of walking and jumping, the frequency of human-induced load was consistent with the first bending frequency of the deck. Whereas the running tests were performed with pedestrian crossing at a pace rate close to 3 Hz. The measurements of accelerations were also taken for a dynamic impact test and using a light vibration exciter. During the impulse tests, a container filled with water with dimensions of $1 \times 1 \times 1$ m was dropped from the height of ca. 6 cm on the footbridges deck. Also, the light vibration exciter was used, which generated a sweep signal with variable frequency in the range of 0–10 Hz. Both tests were repeated in the axis of each hanger in a central axis of a platform. In each test, the measurement time was set in such a way that the suppression of free vibrations of the structure was allowed. In total, 37 dynamic tests were carried out for the footbridge over the S8 road and 38 for the footbridge above the University Route in Bydgoszcz.
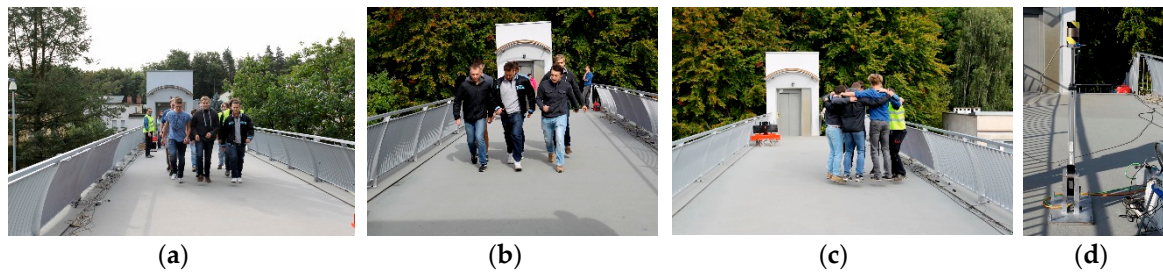
Figure 6. Dynamic excitation methods for the footbridges (**a**) walking; (**b**) running; (**c**) jumping; (**d**) vibration exciter.

2.2.1. Example 1

For the footbridge above S8 expressway, accelerations in twelve points were measured. Eight of them were used to measure the vertical vibrations of the platform, and they were placed in one line sequentially at the beginning of the deck—the first in the axis of the support of the structure, the next near the attachment of all hangers. They were marked with symbols S8_a0z–S8_a7z (see Figure 7). The control vertical and horizontal accelerations were measured on the opposite side of the platform in the axis of attachment of the hanger number 2. During the tests, the horizontal and vertical accelerations of the arch were also captured. The location of all acceleration measuring points during dynamics tests are shown in Figure 7.
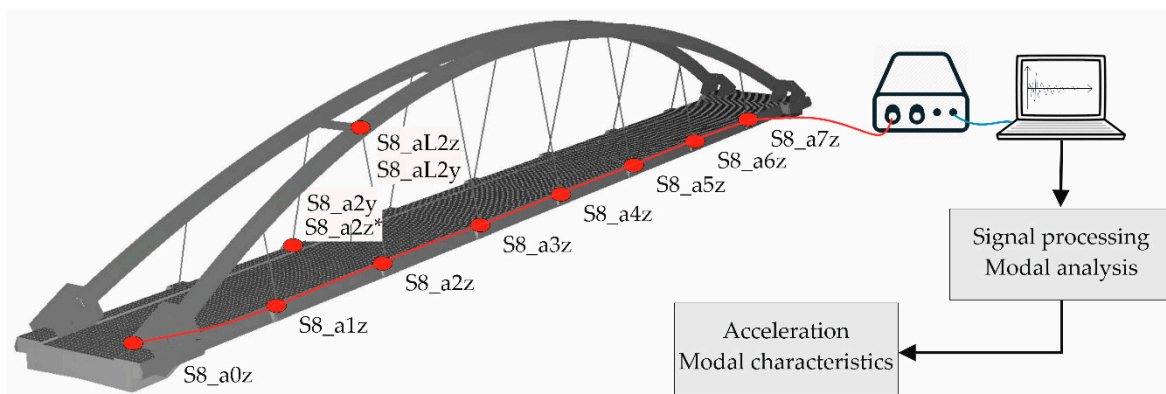

Figure 7. Dynamic measurement scheme of the arch footbridge above expressway S8.

2.2.2. Example 2

A similar set of measurements was conducted for the footbridge above the University Route in Bydgoszcz. In this case, also eight platform accelerations were deployed, starting from the support axis of the structure through the attachment of all hangers. The main measuring points were marked as B_a0z–B_a7z, respectively, as shown in Figure 8. Horizontal and vertical accelerations of the arch were also measured together with accelerations of the opposite side of the deck in the axis of hanger number 2. In addition, the horizontal acceleration of the deck at the attachment of hangers 2 and 5 was measured to assess the maximum horizontal acceleration during human-induced vibrations.
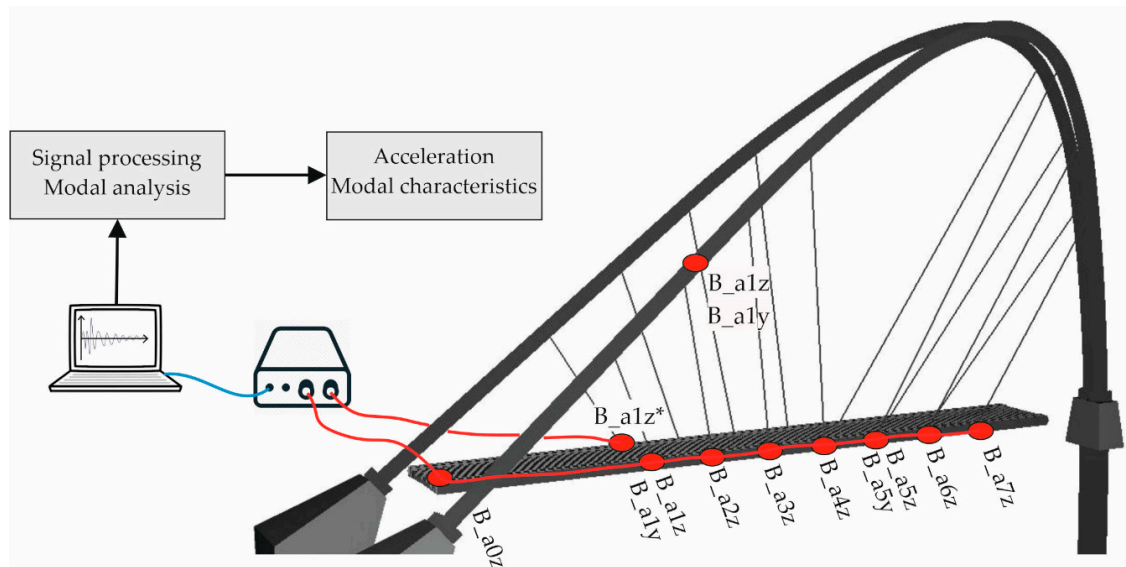
Figure 8. Dynamic measurement scheme of the arch footbridge above the University Route in Bydgoszcz.

2.3. Theory of Experimental Mode Shapes

The methods based on the classical input–output estimation of modal parameters are the well-known and widely used methods of modal analysis [34,35]. The peak picking (PP) method is one of the most accessible because of its simplicity and speed [77,78]. This method is based on the estimation of the frequency response function (FRF) in the frequency domain or the impulse response function (IRF) in the time domain. The experimental tests can be carried out under any excitation, including sinusoidal, impulse, random, or pseudorandom. The excitation is usually applied at one point while the signals are measured at many points. The second method is to place the sensor at one key point of the structure and then force it at subsequent points.

The algorithm of the method assumes subjecting each force signals and structure responses signals to the Fourier transform. Based on the obtained Fourier transform, the transform function $\mathbf{H}(\omega)$ is calculated. In order to receive one row of the matrix $\mathbf{H}(\omega)$, the measurement is taken for the signal of excitation in particular points of the structure; however, the responses are measured in one point. For the matrix column $\mathbf{H}(\omega)$, the signal of force is measured in one point, and the value of structure response is recorded from each measuring point. The determination of mode shapes is possible at any row or matrix column $\mathbf{H}(\omega)$. The measured signals used in the PP method may concern accelerations, velocities, or displacements. The type of signal determines three types of transition functions: accelerance, mobility, and receptance (Table 1).

Table 1. FRFs used in PP method.

FRF	Symbol	Signal
Receptance	$\mathbf{H}^r(\omega)$	$\frac{Displacement}{Force}$
Mobility	$\mathbf{H}^m(\omega)$	$\frac{Velocity}{Force}$
Accelerance	$\mathbf{H}^a(\omega)$	$\frac{Acceleration}{Force}$

The method's limitation is its use for structures that are lightly damped. For structures with very high damping or damping close to zero (infinite peak), the method does not give satisfactory results [78].

The modified PP method can also be used for the operational modal analysis (OMA). In this case, FRF is replaced with power spectrum densities (PDS) from the output. Comparing the results of

PP method with the frequency domain decomposition (FDD) and stochastic subspace identification (SSI), very similar results are usually obtained [39]. Using this method, damping can be estimated by employing the half-power procedure [79].

2.4. Data Processing and Modal Identification

For each of the structures, a series of dynamic tests were carried out. Based on each of them, for each signal from the free response of the structure, the natural frequencies and damping ratios were determined. The final values were obtained by averaging the values from all tests. The linear trend was removed from all time histories, and they were subjected to filtration what allowed us to achieve more satisfactory identification results. In order to remove components from the signal that were beyond the scope of interest, a Butterworth fifth-order filter was used with a cut-off frequency below 0.5 Hz and above 20 Hz [80]. To check the correct operation of all sensors, signals measured during all tests were printed and checked for non-functioning or giving unreal or excessively noisy acceleration values.

2.4.1. Example 1

Figure 9 shows the representative acceleration time histories together with the corresponding normalized fast Fourier transform (FFT) amplitudes for the arch bridge above expressway S8. The excitation in the first case was related to a synchronous march of a group of 12 persons, and in the second case, an impulse caused by dropping a container filled with water was applied. In both cases, the signal was measured at point a5z—vertical composition of the bridge deck acceleration in the axis of hanger number 5.
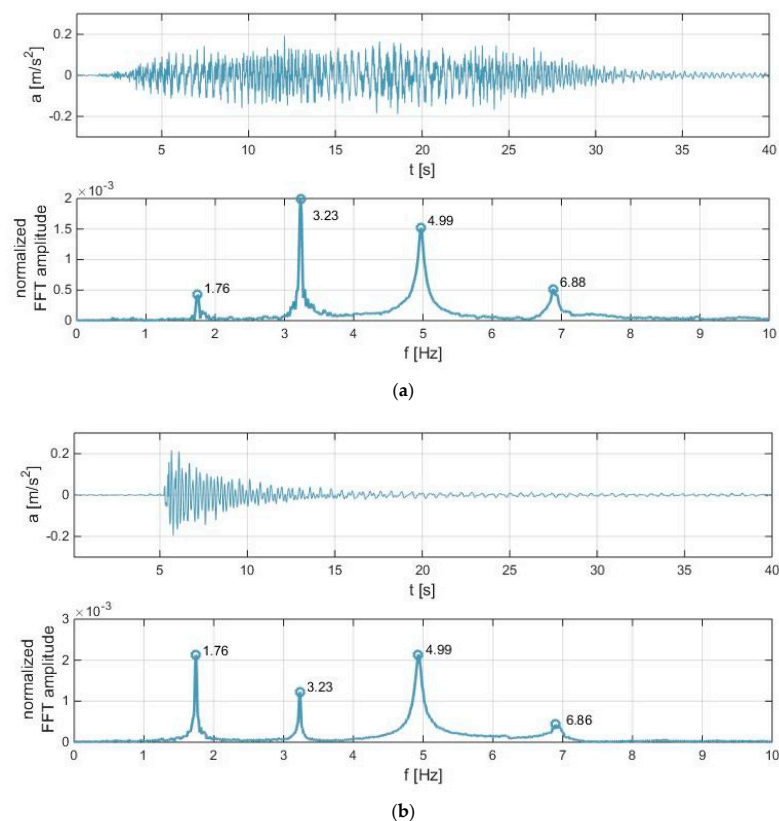

(a)

(b)

Figure 9. Time history of acceleration and normalized FFT amplitude for the arch bridge above expressway S8 at point a5z excited by (**a**) synchronous march of a group of 12 persons, (**b**) impulse.

2.4.2. Example 2

Figure 10 shows the representative acceleration time histories together with the corresponding normalized FFT amplitudes for the footbridge above the University Route in Bydgoszcz (point a1z). Vibrations were caused by the synchronous run of a group of nine persons, and the impulse was induced by dropping a container filled with water. In this case, it was only using impulse excitation it was possible to obtain some frequencies. Neither various types of the human-induced load, as well as the use of a light vibration exciter which generates excitation with a variable frequency, did not allow these frequencies to be identified.
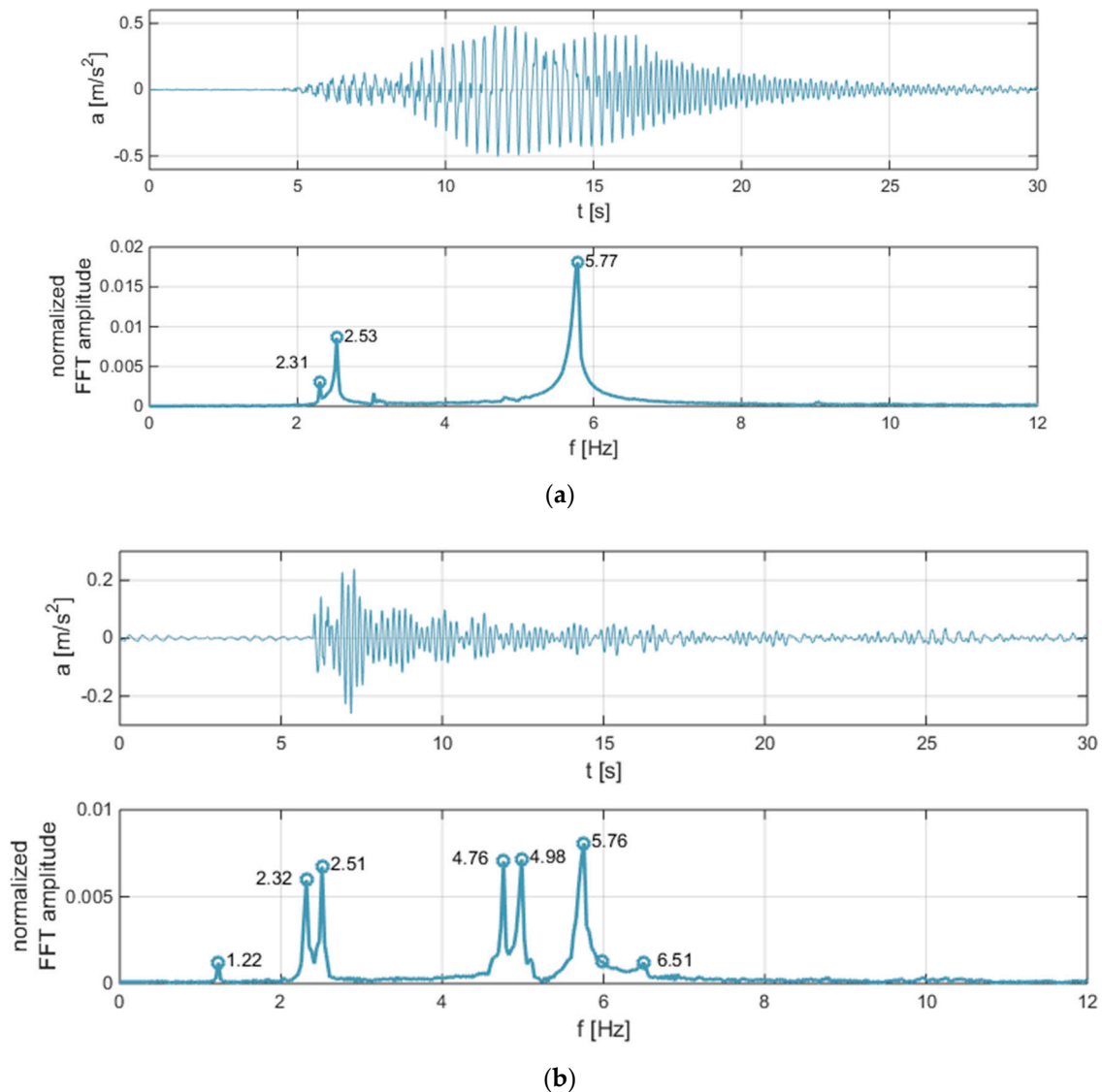

(**a**)

(**b**)

Figure 10. Time history of acceleration and normalized FFT amplitude for the arch footbridge above the University Route in Bydgoszcz at point a1z excited by (**a**) synchronous run of a group of nine persons, (**b**) impulse.

2.5. Finite Element Modeling

In this study, for both footbridges, beam-shell finite element method (FEM) models were constructed using the commercial program SOFiSTiK. These FEM models use four types of finite elements. The decks of both structures were modeled using the two-dimensional, four-nodal (flat) plane finite elements of the Timoshenko–Reissner type (QUAD). These elements have an enriched

state of deformation in the surface, reduction of the blocking effect; they also take into account the shear effect, and the different position of the coating reference surface (eccentric). To model steel girders, one-dimensional, two-node spatial bar (beam) finite elements (BEAM) of the Timoshenko type, taking into account the shear effect and eccentric beam axis, were used. In both models, hangers were modeled using one-dimensional, two-node spatial cable type elements (CABL). To model the retaining blocks supporting the girders of the footbridge in Bydgoszcz, three-dimensional, eight-node solid elements (BRIC), enriched with spatial bending states which further reduce the blocking effect, were used. The piles were also modeled with beam elements (BEAM), taking into account appropriate axial and lateral beddings. The support condition was modeled using linear elastic elements (SPRI), or fully fixed constrains (CONS). Although stiffness of non-structural elements, such as isolation, barriers, and pavement was ignored, their masses were taken into account.

2.5.1. Example 1

The final FEM model (Figure 11) of the footbridge above S8 expressway (after taking into account some elements of FEM convergence analysis) consisted of a grid with 5750 nods, 7008 plane finished elements (QUAD), 682 finished beam elements type BEAM, 14 finished elements type CABL, and 7 elastic elements (SPRI). At the first abutment, one bearing was assumed to be fixed for displacements in all three directions and the second one had only the vertical stiffness. At the second abutment, the sliding type of bearings was assumed with unidirectional and bidirectional slide. The Young's modulus of concrete used in the deck was assumed to be equal to 43 GPa, according to sample test results, and the mass density was equal to 25 kN/m^3.
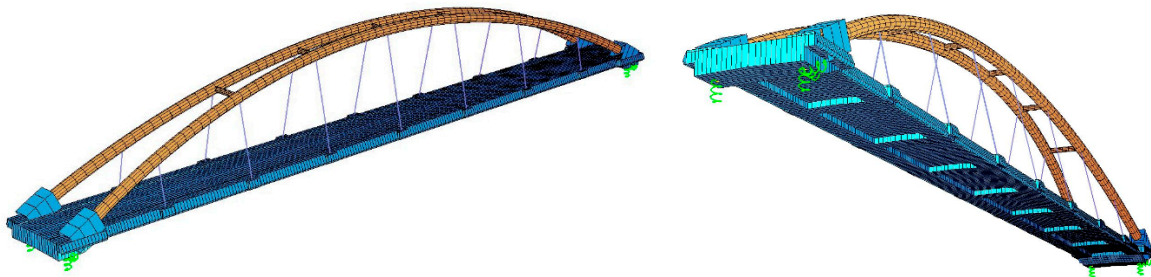

Figure 11. FEM model of the arch footbridge above expressway S8.

2.5.2. Example 2

A detailed model was also developed for the footbridge above the University Route in Bydgoszcz (see Figure 12). After conducting convergence analysis, the final model consisted of 10,904 nodes, 7192 finished elements type QUAD, 968 finished elements type BEAM, 14 finished elements type CABL, 31,108 finished elements type BRICK, and 8 fix constrains. Supports at both ends of the concrete deck were modeled as point supports with free rotations. One bearing at the first abutment was modeled as a fully fixed one, while the other was allowed to slide in the perpendicular direction. On the second abutment, one bearing had a possibility to slide freely in the longitudinal direction and the second one in both directions. The Young's modulus of concrete used in the deck was assumed to be equal to 39 GPa, based on concrete samples test, and the mass density was equal to 25 kN/m^3.

Figure 12. FEM model of the footbridge above University Route in Bydgoszcz.

2.6. Eigenvectors and Eigenvalues

The Lanczos method was chosen to extract the pairs of eigenvectors and eigenvalues from the FEM model in both cases. Due to the geometry of the structures, all designated modes of vibration were marked with symbols and a number, which depended on the type of dominant vibration mode. The symbols Vd, Ld, and Td were used for vertical, lateral, torsional eigenvectors of the deck respectively, and Va and La for the vertical or lateral mode of the arch or steel girder. The symbol is connected with the ratio of the maximum amplitude in the specified direction and normalized with respect to the largest of the components. They also refer directly to the structural element of the footbridges. It indicates that most of the mode shapes are not pure, but they also have other components, which are generally smaller.

2.6.1. Example 1

The first eight eigenvectors identified from the FEM model of the footbridge above S8 expressway together with the corresponding eigenfrequencies are listed in Table 2. At the same time, Figure 13 shows the identified mode shapes of the footbridge. It can be seen that five modes are mainly connected with the deck, and three with the arch. For the modes S8_Vd1, S8_Vd2, S8_Vd3, and S8_Vd4, the component Va is relatively large. It means that the defection of the deck is strictly connected with the deflection of the arch. The same situation occurs in the case of mode S8_Va1. In the modes S8_La1, S8_La2, and S8_Ld1, the other components are much smaller. The numerical model allowed to obtain a higher number of frequencies than was identified during the field test (Figure 9).

Table 2. Modes and eigenvalues identified from the FEM model of the arch bridge above expressway S8.

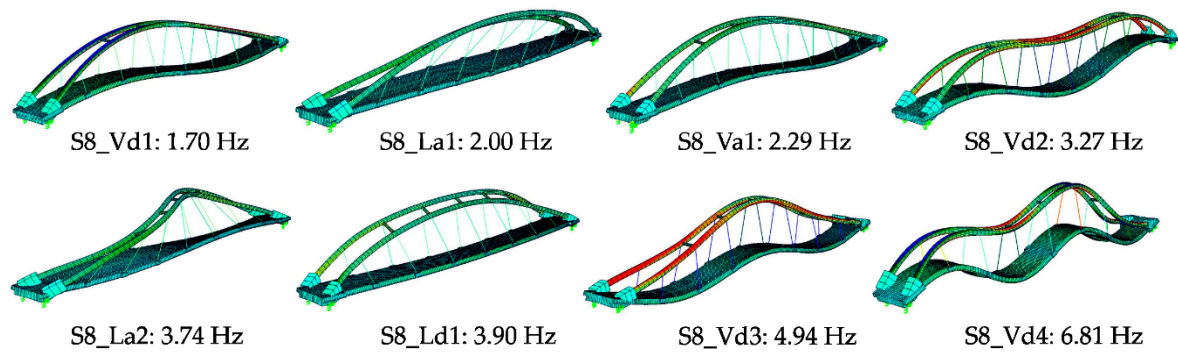| Number	Mode Type	Frequency	Modal Component Ratio				
			Deck			Arch	
		Hz	Vd	Ld	Td	Va	La
1	S8_Vd1	1.70	1.00	0.03	0.00	0.98	0.08
2	S8_La1	2.00	0.14	0.10	0.28	0.14	1.00
3	S8_Va1	2.29	0.95	0.10	0.00	1.00	0.70
4	S8_Vd2	3.27	1.00	0.02	0.00	0.95	0.05
5	S8_La2	3.74	0.13	0.01	0.26	0.08	1.00
6	S8_Ld1	3.90	0.06	1.00	0.00	0.32	0.57
7	S8_Vd3	4.94	1.00	0.03	0.00	0.88	0.16
8	S8_Vd4	6.81	1.00	0.01	0.00	0.95	0.07

Figure 13. FEM model eigenvectors and eigenvalues of the arch footbridge above expressway S8.

2.6.2. Example 2

The first 16 eigenvectors for the footbridge above the University Route in Bydgoszcz together with the corresponding eigenfrequencies are listed in Table 3. The modes of vibration for the structure are shown in Figure 14. In this case, many eigenmodes are typically associated with the arch deflection and low participation of the deck deformation. It can be seen from the Table 3 that eigenvectors B_La1–B_La3, B_La5–B_La7 are rather purely lateral with the movement of steel girder only, while eigenvectors B_La4, B_La8, and B_La9 have significant vertical component as well. Five eigenmodes B_Vd1–B-Vd5 are closely related to the vertical movement of the platform and relatively large deflection of the steel girder have been identified. Among the vertical modes, B_Vd1 have the largest lateral modal component of the steel girder. The two torsional eigenvalues B_Td1 and B_Td2 show the significant bending deflection of the deck. In this case, the platform generally have small horizontal deflection compared to other components for all mode shapes. Despite the use of various excitation techniques during field tests (Figure 10), it was not possible to excite all the vibration frequencies that were obtained in the numerical model.

Table 3. Modes and eigenvalues identified from the FEM model of the arch footbridge above the University Route in Bydgoszcz.

		Frequency	Modal Component Ratio				
			Deck			Arch	
Number	Mode Type	Hz	Vd	Ld	Td	Va	La
1	B_La1	0.94	0.02	0.00	0.00	0.04	1.00
2	B_La2	1.12	0.08	0.00	0.00	0.01	1.00
3	B_La3	2.30	0.05	0.01	0.00	0.13	1.00
4	B_Vd1	2.35	1.00	0.01	0.00	0.66	0.73
5	B_La4	2.65	0.43	0.00	0.00	0.51	1.00
6	B_La5	3.39	0.07	0.01	0.00	0.20	1.00
7	B_Vd2	3.58	1.00	0.02	0.00	0.89	0.40
8	B_La6	4.01	0.13	0.00	0.00	0.08	1.00
9	B_La7	4.17	0.09	0.01	0.00	0.14	1.00
10	B_Vd3	4.82	1.00	0.01	0.00	0.72	0.12
11	B_Td1	4.95	0.50	0.01	1.00	0.33	0.11
12	B_Td2	5.18	0.49	0.03	1.00	0.42	0.24
13	B_La8	5.26	0.29	0.01	0.00	0.14	1.00
14	B_La9	5.27	0.31	0.02	0.58	0.14	1.00
15	B_Vd4	5.56	1.00	0.03	0.00	0.97	0.16
16	B_Vd5	5.90	1.00	0.01	0.00	0.51	0.17

B_La1: 0.94 Hz B_La2: 1.12 Hz B_La3: 2.30 Hz B_Vd1: 2.35 Hz

B_La4: 2.65 Hz B_La5: 3.39 Hz B_Vd2: 3.58 Hz B_La6: 4.01 Hz

B_La7: 4.17 Hz B_Vd3: 4.82 Hz B_Td1: 4.95 Hz B_Td2: 5.18 Hz

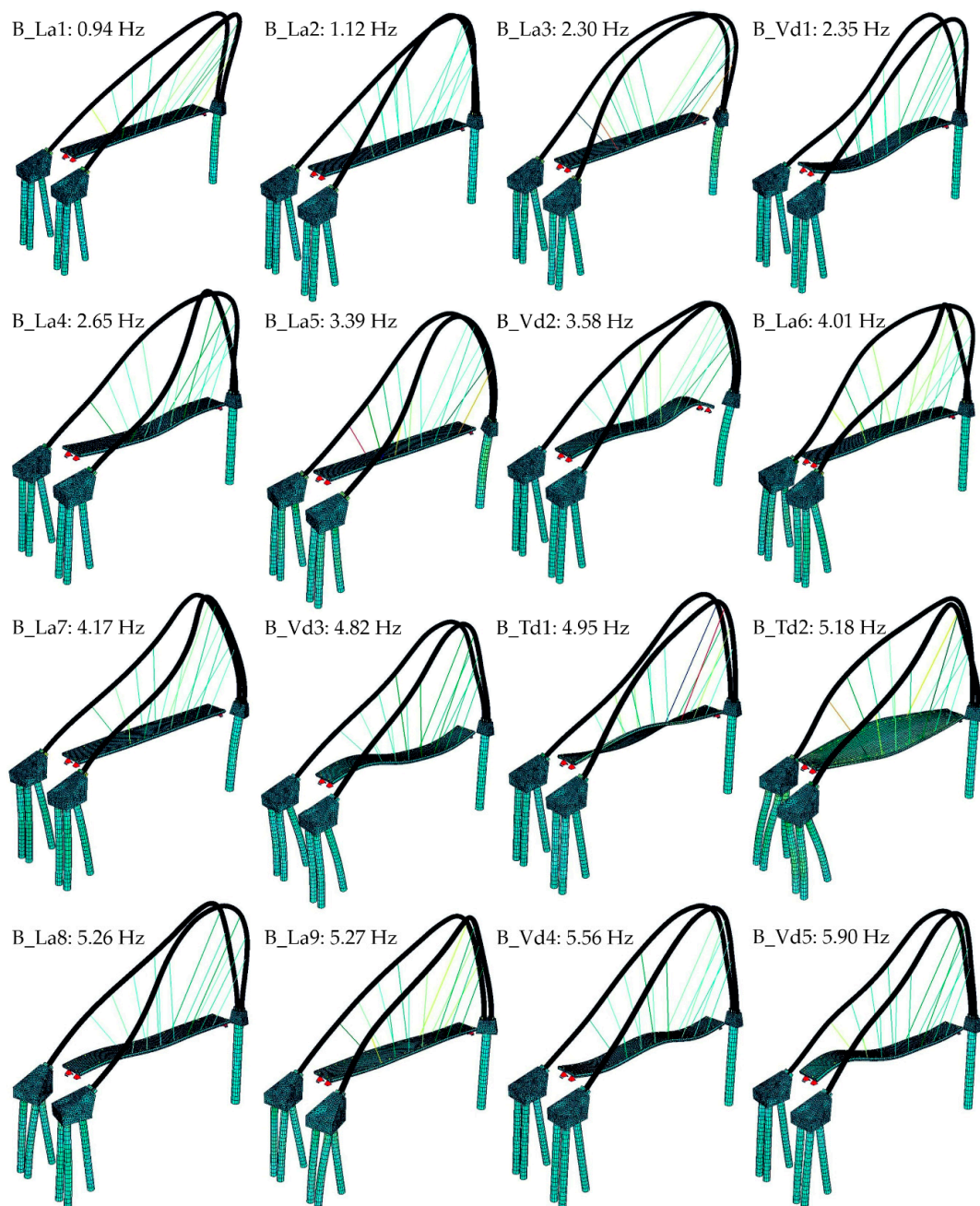B_La8: 5.26 Hz B_La9: 5.27 Hz B_Vd4: 5.56 Hz B_Vd5: 5.90 Hz

Figure 14. FEM eigenvectors and eigenvalues of the footbridge above the University Route in Bydgoszcz.

2.7. Theory of Mode Shapes and Frequencies Validation Criteria

The combination of modal pairs, i.e. frequencies and modal shapes, creates a representation of the basic dynamic properties of the structure. Mode shapes can be the basis for many further analyses, such as validation or updating of numerical models. Thus, they enable the assessment of the condition of the structure or are the basis for diagnostic analyses.

Conducting advanced analyses based on comparing dynamic characteristics determined in experimental research of real structure and characteristics obtained as a result of numerical analyses requires the use of appropriate comparative techniques. One of the most significant problems is related to the 'pairing' mode shapes, both in terms of frequencies and mode shapes. This concerns particularly more complex structures, for which modal shapes may seem to be similar. Another important issue is

the difference in scale of the amplitude of the modal shapes obtained from the numerical model and experimental studies.

Modal assurance criterion (MAC) is one of the most popular criteria which is often used for comparing the mode shapes of free vibrations [81]. It can be defined as

$$\text{MAC}_{ij} = \frac{\left|\Phi_{mi}^T \Phi_{aj}\right|^2}{\left(\Phi_{aj}^T \Phi_{aj}\right)\left(\Phi_{mi}^T \Phi_{mi}\right)} \tag{1}$$

where Φ_{mj} Φ_{aj} are the experimental and numerical mode shapes, respectively, and symbol T denotes the transposition.

The criterion compares only the mode shapes, which means that it is necessary to simultaneously use the criterion of comparing the natural frequencies. The result is a MAC matrix in which the elements take values between zero (no match) and one (complete match). This presentation allows us, together with the frequency comparison, to select the appropriate modal pairs from experimental study and numerical analysis. When the MAC value is greater than 0.90, it is assumed that the compatibility of mode shapes is high [50,66].

The MAC criterion was introduced together with the modal scale factor (MSF), which is the scaling factor for the mode shapes obtained from experimental tests in relation to the parameter obtained from numerical analyses. The coefficient is expressed by the formula

$$\text{MSF}_i = \frac{\Phi_{ai}^T \Phi_{mi}}{\Phi_{mi}^T \Phi_{mi}} \tag{2}$$

The difference between experimental and numerical frequencies can be defined as

$$\Delta f = \frac{f_a - f_m}{f_m} \cdot 100 [\%] \tag{3}$$

where f_m f_a are the experimental and numerical frequencies, respectively.

2.8. Footbridge Classification According to Current Codes

The French Sétra guidelines [24] and the European guidelines "Human-induced vibration of steel structures" (HiVoss) [25] are the two most commonly used documents regarding pedestrian comfort on the footbridges. The first one applies to all structures regardless of the material, the second concerns only steel structures. The perception of vibrations is very subjective. It depends, among others, on their duration and direction of vibrations, as well as human activity and position [82]. For this reason, there are always difficulties in developing versatile comfort guidelines. Both Sétra and HiVoss guidelines propose to introduce four comfort levels (Figure 15). In the case of vertical vibrations, the boundaries between the levels are the same and are equal to 0.5 m/s^2, 1 m/s^2, and 2.5 m/s^2 for the maximum, mean, and minimum comfort, respectively. Accelerations exceeding the vertical value of 2.5 m/s^2 are considered as unacceptable. The level of horizontal vibrations should take into account the lock-in effect. It is assumed that, in the case of the accelerations of structures smaller than 0.1 m/s^2 according to Sétra and 0.15 m/s^2 according to HiVoss, the lock-in effect will not occur due to random load charter and lack of synchronization of pedestrians. Horizontal accelerations exceeding the value of 0.8 m/s^2 are considered as unacceptable.
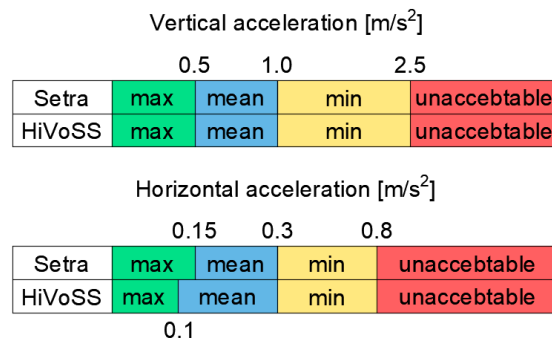
Figure 15. Comfort levels and corresponding acceleration ranges according to Serta and HiVoSS.

3. Results and Discussion

3.1. Comparison between the Experimental and Numerical Results

In order to verify the accuracy and validate the FEM models of both footbridges, comparisons of the dynamic structural properties were conducted, based on experimental and numerical results [39]. In both cases, the mode shapes were obtained by measuring the accelerations at all points of the footbridge. While the excitations were always applied and measured at one point of the deck. Due to the relatively low mass of the container filled with water and vibration exciter, they did not affect the frequencies and the mode shapes obtained. On this basis, FRF was calculated, which using the PP method was used to determine the mode shapes. The damping was determined using the HPM method.

3.1.1. Example 1

The identified mode shapes obtained from the field tests and numerical analysis for the footbridge above the expressway S8 are presented in Figure 16a. Additionally, the representation of MAC matrix between the FEM model and filed test mode shapes is shown in Figure 16b. The identified mode shapes correspond to all eigenvectors marked as Vd from the numerical model presented in the spatial drawing in Figure 13. The field tests allowed us to identify all mode shapes associated with the significant vertical movement of the deck. The lack of detection of frequencies related to the movement of the arch is due to the lack of sufficient excitation that would cause correspondingly large vibrations of the arc structure. A comparison between the experimentally and numerically obtained frequencies, together with the corresponding damping ratios and MACs of the arch bridge above the expressway S8, are shown in Table 4. It can be seen from the table that the vertical frequencies have a relatively low-frequency error, less than 3.5 %. Based on the literature examples [22,39,47,83] differences in the received frequencies were considered satisfactory. Also, modes Vd1, Vd2, Vd3, and Vd4 mode shapes of the FEM model correspond to the experimentally identified modes. This is demonstrated by the MAC values of 0.99 for each mode. The graphical representation of the MAC matrix (Figure 16b) shows that the identified mode shapes correspond exactly to the coincidence of the eigenvalues from the FEM model.
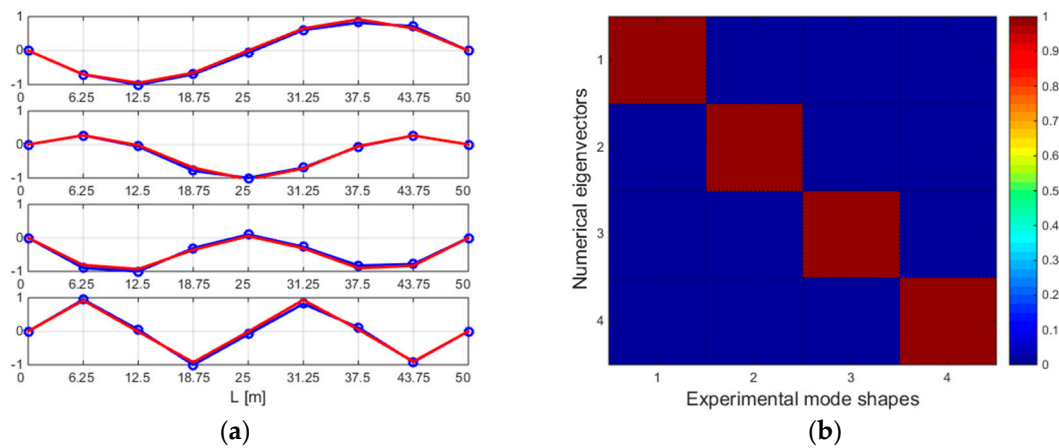
Figure 16. (**a**) Comparison of experimental vertical mode shapes (field test—blue; FEM model—red) (**b**) Representation of MAC matrix between the FEM model and filed test mode shapes of the arch bridge above expressway S8.

Table 4. Correlation between experimental and FEM model modal parameters of the arch bridge above expressway S8.

Mode	Frequency (Hz)		Relative Difference (%)	Damping Ratio (%)	MAC (-)
	Field Test	FEM Model	Δf	ξ	Impulse
Vd1	1.76	1.70	3.5	4.2	0.99
Vd2	3.23	3.27	−1.2	0.4	0.99
Vd3	4.99	4.94	1.0	0.7	0.99
Vd4	6.86	6.81	0.7	1.2	0.99

3.1.2. Example 2

A comparison between the experimentally and numerically obtained frequencies, together with the corresponding damping ratios and MACs of the arch bridge above the University Route in Bydgoszcz, are shown in Table 5. The mode shapes are also displayed in Figures 17a and 18a depending on the type of excitation. Additionally, the representations of MAC matrix between the FEM model and filed test mode shapes are shown in Figures 17b and 18b. The identified vibrations correspond to the first and the fifth bending modes of the deck marked as B_Vd1 and B_Vd5 of the FEM model. Torsional mode shapes B_Td1 and B_Td2 were also determined with high accuracy. It was also possible to accurately identify the La4 mode shape, which was characterized by a relatively high coefficient of vertical vibration of the deck. It can be concluded on the basis of created MAC matrices (Figures 17b and 18b) that the first four mode shapes are characterized by a high similarity. Almost identical shapes of vibrations occurred for pairs of vibrations B_Vd1 and B_La4 as well as B_Td1 and B_Td2 with close frequencies. Despite the sinusoidal signal with variable frequency, the third mode shape could not be identified using a vibration exciter. The other four mode shapes were identified with high compliance and MAC value greater than 0.97. With the impulse excitation, five mode shapes were obtained with high accuracy and MAC value close to 1. However, the vertical mode shapes of platform vibration B_Vd2–B_Vd4 could not be identified. Despite various methods of excitation of the structure, including excitation with a sinusoidal signal with variable frequency, it was not possible to determine the frequencies corresponding to these mode shapes. The frequencies of the FEM model provided a fairly good approximation of the actual footbridge frequencies (Table 3). The largest discrepancies (but still close to 5%) were obtained for the fifth mode.

Table 5. Correlation between experimental and FEM model modal parameters of the arch bridge above the University Route in Bydgoszcz.

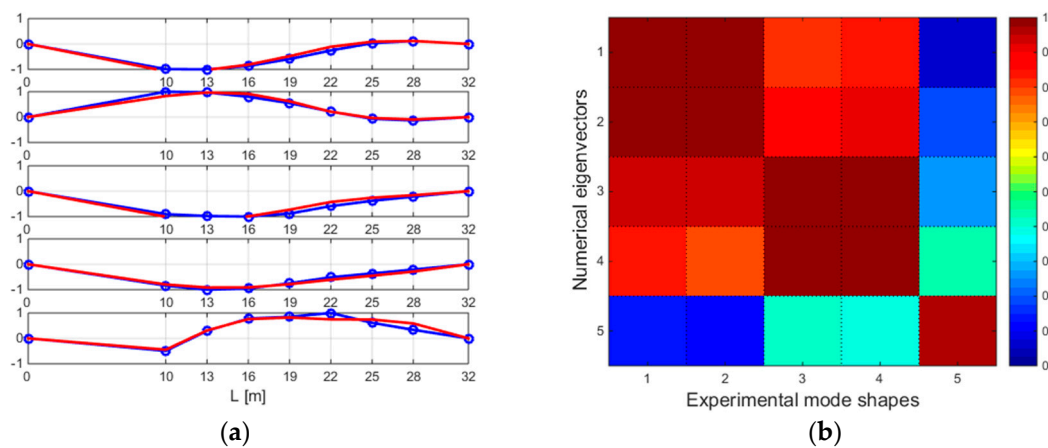| Mode	Frequency (Hz)		Relative Difference (%)	Damping Ratio (%)	MAC (-)	
	Field Test	FEM Model	Δf	ξ	Impulse	Vibration Exciter
B_Vd1	2.31	2.35	1.7	1.3	0.99	1.00
B_La4	2.52	2.65	5.2	0.5	0.99	1.00
B_Td1	4.77	4.95	3.8	2.1	0.99	-
B_Td2	4.99	5.18	3.8	1.1	0.99	0.99
B_Vd5	5.73	5.90	3.0	0.6	0.95	0.97

(a)   (b)

Figure 17. (**a**) Comparison of experimental vertical mode shapes (field test—blue; FEM model—red). (**b**) Representation of MAC matrix between the FEM model and filed test mode shapes of the arch bridge above the University Route in Bydgoszcz.

(a)   (b)

Figure 18. (**a**) Comparison of experimental vertical mode shapes (field test—blue; FEM model—red). (**b**) Representation of MAC matrix between the FEM model and filed test mode shapes of the arch footbridge above the University Route in Bydgoszcz.
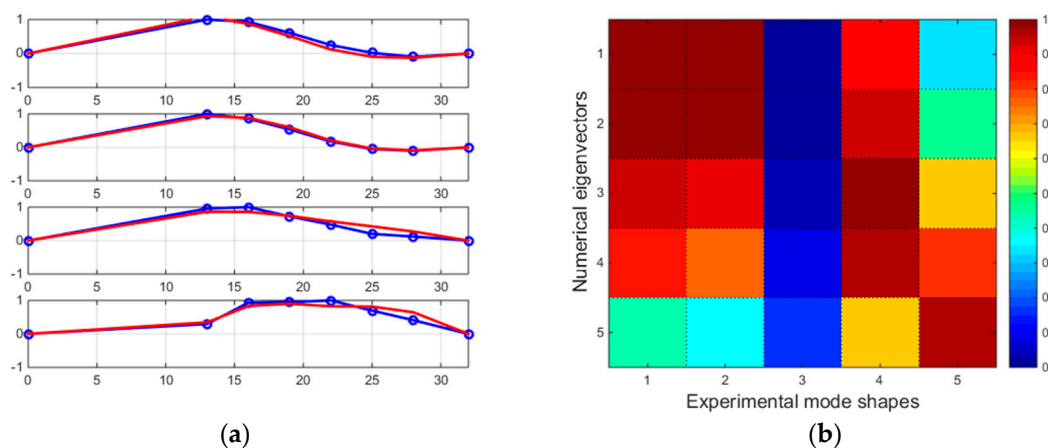
3.2. Assessment of Pedestrian Effects

The conducted experimental tests and numerical analyses confirm the occurrence of resonance frequencies similar to the human-induced loading. Thus, there is a risk of resonance concerning both structures. In this case, the comfort of pedestrians on both structures was only assessed after they were built based on accelerations obtained during field tests. In order to estimate the level of

accelerations, that may appear during exploitation on the footbridges, series of dynamic field tests under human-induced loading were carried out. However, it seems reasonable to conduct such analyses at the design stage and introduce possible modifications to the structure in case of excessive vibration. Tables 6 and 7 show the peak acceleration level for each measuring point.

Table 6. Peak recorded acceleration due to human-induced loading acting on the arch bridge above expressway S8.

Sensor	Walk				Run				Jump
	Synchronous		Free		Synchronous		Free		Synch.
	6 ped.	12 ped.	6 ped.	12 ped.	6 ped.	12 ped.	6 ped.	12 ped.	6 ped.
	Vertical acceleration (m/s^2)								
a1z	0.21	0.31	0.13	0.12	0.21	0.25	0.11	0.12	0.36
a2z	0.20	0.31	0.17	0.14	0.20	0.23	0.13	0.15	0.43
a3z	0.24	0.31	0.13	0.14	0.40	0.48	0.13	0.15	0.48
a4z	0.14	0.22	0.05	0.06	0.37	0.53	0.13	0.20	0.48
a5z	0.20	0.28	0.11	0.12	0.30	0.42	0.11	0.14	0.39
a6z	0.18	0.30	0.15	0.14	0.18	0.21	0.12	0.12	0.40
a7z	0.23	0.32	0.13	0.12	0.15	0.20	0.12	0.13	0.36
	Horizontal acceleration (m/s^2)								
a2y	0.02	0.02	0.01	0.01	0.02	0.02	0.01	0.01	0.3

Table 7. Peak recorded acceleration due to human-induced loading acting on the arch bridge above University Route in Bydgoszcz.

Sensor	Walk					Run					Jump	
	Synchronous			Free		Synchronous			Free		Sync	Free
	6	9	12	6	12	6	9	12	6	12	6	12
	Vertical acceleration (m/s^2)											
a1z	0.93	1.83	1.19	0.05	0.07	0.42	0.58	0.62	0.22	0.48	1.24	2.16
a2z	0.83	1.84	1.08	0.09	0.08	0.45	0.68	0.59	0.23	0.37	1.31	2.23
a3z	0.72	1.49	0.93	0.06	0.07	0.41	0.65	0.70	0.21	0.40	1.12	1.59
a4z	0.91	1.83	1.14	0.05	0.04	0.35	0.56	0.55	0.22	0.40	1.17	2.20
a5z	0.40	1.12	0.50	0.07	0.08	0.31	0.50	0.39	0.13	0.18	0.73	1.16
a6z	0.35	0.75	0.41	0.05	0.05	0.29	0.37	0.37	0.12	0.17	0.71	0.80
a7z	0.34	0.59	0.46	0.07	0.03	0.30	0.29	0.29	0.09	0.12	0.53	0.57
	Horizontal acceleration (m/s^2)											
a1y	0.18	0.19	0.16	0.01	0.01	0.08	0.09	0.11	0.03	0.06	0.22	0.37
a5y	0.13	0.24	0.17	0.02	0.02	0.12	0.13	0.13	0.04	0.05	0.31	0.26

3.2.1. Example 1

For the arch bridge above expressway S8, all accelerations were characterized generally with a vertical acceleration value of less than 0.5 m/s^2 (see Table 6). The peak acceleration value was equal to 0.53 m/s^2, and it occurred for the synchronic run of a group of 12 persons. It was the only case when the accelerations exceeded the limit value for the first-class level according to Sétra guidelines [24]. For the march, the peak accelerations were usually in the quarter, while they were much smaller in the middle of the span because walkers excite mainly the first mode. A different situation was due to running. When running at a frequency close to 3.0 Hz, peak acceleration occurred in the center of the deck, which corresponds to the second mode shape. The level of horizontal vibrations was negligibly small and did not exceed the recommended values in [24].

3.2.2. Example 2

In the case of the arch footbridge above the University Route in Bydgoszcz, the peak acceleration values were much higher (see Table 7). The highest accelerations occurred for the synchronous march.

It was induced by a group of nine persons with a value equal to 1.84 m/ s^2. However, increasing the number of pedestrians did not increase the acceleration level; instead, its reduction was observed. This is due to difficulties with ensuring synchronization among pedestrians with larger groups. Lower acceleration levels occurred for the run. It was caused by the frequency of excitation, which is not close to any of the bridge's natural vibrations. The peak acceleration values, irrespective of the type of excitation, occurred in the part where the steel girder was lower above the deck. This is due to the lower stiffness of the structure, and thus the occurrence of the maximum amplitude of first four mode shapes in this area. The horizontal levels of the deck acceleration were significantly smaller than vertical ones, but they could not be considered negligible. For synchronic excitations, they correspond to the mean level of comfort, and even to the minimal level of comfort for jumps. It is worth mentioning that acceleration levels were significantly lower for unsynchronized pedestrian groups. They did not exceed the value of 0.23 m/s^2 for vertical vibrations and of 0.06 m/s^2 for horizontal ones. The footbridge exhibited a high level of comfort during normal exploitation according to Sétra guidelines [24] (Figure 15); however, the classification of comfort would be different in the case of intentional or vandalized excitations.

4. Conclusions

The experimental and numerical results of the dynamic system identification and verification of the behavior of two footbridges in Poland have been presented in this paper. The study has concerned the footbridge above the S8 expressway, and the structure above the University Route in Bydgoszcz. The vibration testing altogether with the system identification and correlation techniques have been applied in the study.

Firstly, experimental tests under different scenarios of human-induced load, impulse load, and excitations induced by vibration exciter, have been conducted. The results obtained show that it is possible to detect all four bending mode shapes, and the corresponding natural frequencies, of the deck for the footbridge above S8 expressway in the case of impulse excitation. Moreover, the study proves that for a footbridge above the University Route in Bydgoszcz, only the test with the use of impulse excitation allows the identification of five frequencies that have not been triggered by any other excitation (human-induced load or using a vibration exciter). The results of the tests indicate that both structures under investigation have the first bending frequency of the deck in the range of human-induced excitation. Therefore, there is a risk of excessive structural vibrations during exploitation.

In the second stage of the study, numerical analyses have been carried out. The detailed FEM models, based on technical drawings, have successfully matched the experimentally identified modal parameters of the footbridges. The comparison between experimental and numerical results show a good agreement, both in the case of frequencies and mode shapes, with the MAC value close to one.

Finally, the vibration serviceability of footbridges has been assessed according to the current codes of practice. The footbridge over the S8 expressway, regardless of the scenario of human-induced loading (even with excitations that can be considered as vandalistic), provides a maximum level of comfort to its users. Different situation concerns the footbridge above the University Route in Bydgoszcz. This time, the accelerations measured under synchronized walking, running, and jumping scenarios have exceeded comfort level, even for a small group of pedestrians. The results of the study show that this structure meets the assumptions of the guidelines for vibration severability in normal use; nevertheless, it is susceptible to excitations induced by synchronized users, even in the case of a small group of pedestrians.

It should be added that, once the footbridge has been constructed, it is recommended to conduct dynamic field tests, especially if the frequencies determined from the numerical model at the design stage are similar to the human-induced loading. The identified dynamic parameters can be further used to update the numerical model. Then, the updated numerical model can be employed to carry

out the extensive numerical analyses focused on the response of structures under different dynamic loads, including wind and earthquakes.

References

1. Maciag, E.; Kuzniar, K.; Tatara, T. Response Spectra of Ground Motions and Building Foundation Vibrations Excited by Rockbursts in the LGC Region. *Earthq. Spectra* **2016**, *32*, 1769–1791. [CrossRef]
2. Elwardany, H.; Seleemah, A.; Jankowski, R. Seismic pounding behavior of multi-story buildings in series considering the effect of infill panels. *Eng. Struct.* **2017**, *144*, 139–150. [CrossRef]
3. Falborski, T.; Jankowski, R. Experimental Study on Effectiveness of a Prototype Seismic Isolation System Made of Polymeric Bearings. *Appl. Sci.* **2017**, *7*, 808. [CrossRef]
4. Miari, M.; Choong, K.K.; Jankowski, R. Seismic pounding between adjacent buildings: Identification of parameters, soil interaction issues and mitigation measures. *Soil Dyn. Earthq. Eng.* **2019**, *121*, 135–150. [CrossRef]
5. Sołtysik, B.; Jankowski, R. Non-linear strain rate analysis of earthquake-induced pounding between steel buildings. *Int. J. Earth Sci. Eng.* **2013**, *6*, 429–433.
6. Kuzniar, K.; Tatara, T. The ratio of response spectra from seismic-type free-field and building foundation vibrations: The influence of rockburst parameters and simple models of kinematic soil-structure interaction. *Bull. Earthq. Eng.* **2020**, *18*, 907–924. [CrossRef]
7. Drygala, I.J.; Polak, M.A.; Dulinska, J.M. Vibration serviceability assessment of GFRP pedestrian bridges. *Eng. Struct.* **2019**, *184*, 176–185. [CrossRef]
8. Flaga, A. *Footbridges*; WKŁ: Warsaw, Poland, 2011.
9. Živanović, S.; Pavic, A.; Reynolds, P. Vibration serviceability of footbridges under human-induced excitation: A literature review. *J. Sound Vib.* **2005**, *279*, 1–74. [CrossRef]
10. Dallard, P.; Fitzpatrick, T.; Flint, A.; Bourva, S.; Low, A.; Ridsdill, R.; Willford, M. The London Millennium Footbridge. *Struct. Eng.* **2001**, *79*, 17–33.
11. Dallard, P.; Fitzpatrick, T.; Flint, A.; Low, A.; Smith, R.R.; Willford, M.; Roche, M. London Millennium Bridge: Pedestrian-Induced Lateral Vibration. *J. Bridge Eng.* **2001**, *6*, 412–417. [CrossRef]
12. Dallard, P. Pedestrian Excitation on the London Millennium Footbridge. *Struct. Congr.* **2005**, 1–13. [CrossRef]
13. Dziuba, P.; Grillaud, G.; Flamand, O.; Sanquier, S.; Tétard, Y. La passerelle Solférino. Comportement dynamique. *Bull. Ouvrages Métall.* **2001**, *1*, 34–57.
14. Blekherman, A.N. Autoparametric Resonance in a Pedestrian Steel Arch Bridge: Solferino Bridge, Paris. *J. Bridge Eng.* **2007**, *12*, 669–676. [CrossRef]
15. Caetano, E.; Cunha, Á.; Magalhães, F.; Moutinho, C. Studies for controlling human-induced vibration of the Pedro e Inês footbridge, Portugal. Part 1: Assessment of dynamic behavior. *Eng. Struct.* **2010**, *32*, 1069–1081. [CrossRef]
16. Caetano, E.; Cunha, Á.; Moutinho, C.; Magalhães, F. Studies for controlling human-induced vibration of the Pedro e Inês footbridge, Portugal. Part 2: Implementation of tuned mass dampers. *Eng. Struct.* **2010**, *32*, 1082–1091. [CrossRef]
17. Živanović, S.; Pavic, A.; Reynolds, P. Modal testing and FE model tuning of a lively footbridge structure. *Eng. Struct.* **2006**, *28*, 857–868. [CrossRef]
18. Salgado, R.; Branco, J.M.; Cruz, P.J.S.; Ayala, G. Serviceability assessment of the Góis footbridge using vibration monitoring. *Case Stud. Nondestruct. Test. Eval.* **2014**, *2*, 71–76. [CrossRef]
19. Nakamura, S.; Kawasaki, T. Lateral vibration of footbridges by synchronous walking. *J. Constr. Steel Res.* **2006**, *62*, 1148–1160. [CrossRef]

20. Piccardo, G.; Tubino, F. Simplified procedures for vibration serviceability analysis of footbridges subjected to realistic walking loads. *Comput. Struct.* **2009**, *87*, 890–903. [CrossRef]

21. Van Nimmen, K.; Lombaert, G.; De Roeck, G.; Van den Broeck, P. Vibration serviceability of footbridges: Evaluation of the current codes of practice. *Eng. Struct.* **2014**, *59*, 448–461. [CrossRef]

22. Lai, E.; Gentile, C.; Mulas, M.G. Experimental and numerical serviceability assessment of a steel suspension footbridge. *J. Constr. Steel Res.* **2017**, *132*, 16–28. [CrossRef]

23. Bassoli, E.; Gambarelli, P.; Vincenzi, L. Human-induced vibrations of a curved cable-stayed footbridge. *J. Constr. Steel Res.* **2018**, *146*, 84–96. [CrossRef]

24. Sétra/Afgc. *Sétra Technical Guide Footbridges Assessment of Vibrational Behavior of Footbridges under Pedestrian Loading*; Sétra/Afgc: Paris, France, 2006.

25. Feldmann, M. *Human-Induced Vibration of Steel Structures (Hivoss): Designing of Footbridges*; Reaserch Fund for Coal and Steel; Publications Office of the European Union: Luxembourg, 2010.

26. Brownjohn, J.; Fok, P.; Roche, M.; Moyo, P. Long span steel pedestrian bridge at Singapore Changi Airport—Part 1: Prediction of vibration serviceability problems. *Struct. Eng.* **2004**, *82*, 21–27.

27. Brownjohn, J.; Fok, P.; Roche, M.; Omenzetter, P. Long span steel pedestrian bridge at Singapore Changi Airport—Part 2: Crowd loading tests and vibration mitigation measures. *Struct. Eng.* **2004**, *82*, 28–34.

28. Butz, C.; Schürmann, C.J.; Benicke, O.S. Tuned Mass Dampers for the Footbridge of VW Autostadt in Wolfsburg, Germany. In Proceedings of the 4th international footbridge conference, Wroclaw, Poland, 6–8 July 2011.

29. Ainsworth, I.; Franklin, K.; Burnton, P. Kurilpa Bridge—A Case Study. In Proceedings of the 4th International Footbridge Conference, Wroclaw, Poland, 6–8 July 2011; p. 1.

30. Xu, X.; Li, Z.; Liu, W.; Feng, D.; Li, X. Investigation of the wind-resistant performance of seismic viscous dampers on a cable-stayed bridge. *Eng. Struct.* **2017**, *145*, 283–292. [CrossRef]

31. Preumont, A.; Voltan, M.; Sangiovanni, A.; Mokrani, B.; Alaluf, D. Active Tendon Control of Suspension Bridges. *Smart Struct. Syst.* **2015**, *18*. [CrossRef]

32. Aktan, A.E.; Brownjohn, J.M.W. Structural Identification: Opportunities and Challenges. *J. Struct. Eng.* **2013**, *139*, 1639–1647. [CrossRef]

33. Zhou , Y.; Zhang, J.; Yi, W.; Jiang, Y.; Pan, Q. Structural Identification of a Concrete-Filled Steel Tubular Arch Bridge via Ambient Vibration Test Data. *J. Bridge Eng.* **2017**, *22*, 04017049. [CrossRef]

34. Maia, N.M.M.; Silva, J.M.M. *Theoretical and Experimental Modal Analysis*; Research Studies Press: Letchworth, UK, 1997.

35. Ewins, D.J. *Modal Testing: Theory, Practice, and Application*; Research Studies Press: Letchworth, UK, 2000; ISBN 978-0-86-380218-8.

36. Heylen, W.; Lammens, S.; Sas, P. *Modal Analysis Theory and Testing*; Katholieke Universiteit Leuven: Leuven, Belgium, 2007; ISBN 978-9-07-380261-2.

37. Ali, A.; Sandhu, T.Y.; Usman, M. Ambient Vibration Testing of a Pedestrian Bridge Using Low-Cost Accelerometers for SHM Applications. *Smart Cities* **2019**, *2*, 20–30. [CrossRef]

38. Tomaszewska, A.; Szafrański, M. Study on applicability of two modal identification techniques in irrelevant cases. *Arch. Civ. Mech. Eng.* **2020**, *20*, 13. [CrossRef]

39. Chen, G.-W.; Omenzetter, P.; Beskhyroun, S. Operational modal analysis of an eleven-span concrete bridge subjected to weak ambient excitations. *Eng. Struct.* **2017**, *151*, 839–860. [CrossRef]

40. Brincker, R.; Zhang, L.; Andersen, P. Modal identification of output-only systems using frequency domain decomposition. *Smart Mater. Struct.* **2001**, *10*, 441–445. [CrossRef]

41. Xiong, C.; Lu, H.; Zhu, J. Operational Modal Analysis of Bridge Structures with Data from GNSS/Accelerometer Measurements. *Sensors* **2017**, *17*, 436. [CrossRef] [PubMed]

42. Jr, R.R.C.; Kurdila, A.J. *Fundamentals of Structural Dynamics*; John Wiley & Sons: Hoboken, NJ, USA, 2011; ISBN 978-1-11-817444-9.

43. Peeters, B.; Roeck, G.D. Reference based stochastic subspace identification in civil engineering. *Inverse Probl. Eng.* **2000**, *8*, 47–74. [CrossRef]

44. Juang, J.-N.; Pappa, R.S. An eigensystem realization algorithm for modal parameter identification and model reduction. *J. Guid. ControlDyn.* **1985**, *8*, 620–627. [CrossRef]

45. Peeters, B.; Ventura, C.E. Comparative Study of Modal Analysis Techniques for Bridge Dynamic Characteristics. *Mech. Syst. Signal Process.* **2003**, *17*, 965–988. [CrossRef]

46. Peeters, B.; De Roeck, G. Stochastic System Identification for Operational Modal Analysis: A Review. *J. Dyn. Sys. Meas. Control* **2001**, *123*, 659–667. [CrossRef]

47. Drygala, I.J.; Dulinska, J.M. Full-Scale Experimental and Numerical Investigations on the Modal Parameters of a Single-Span Steel-Frame Footbridge. *Symmetry* **2019**, *11*, 404. [CrossRef]

48. Ren, W.-X.; Zong, Z.-H. Output-only modal parameter identification of civil engineering structures. *Struct. Eng. Mech.* **2004**, *17*, 429–444. [CrossRef]

49. Kvåle, K.A.; Øiseth, O.; Rønnquist, A. Operational modal analysis of an end-supported pontoon bridge. *Eng. Struct.* **2017**, *148*, 410–423. [CrossRef]

50. Živanović, S.; Pavic, A.; Reynolds, P. Finite element modeling and updating of a lively footbridge: The complete process. *J. Sound Vib.* **2007**, *301*, 126–145. [CrossRef]

51. Jaishi, B.; Ren, W.-X. Finite element model updating based on eigenvalue and strain energy residual using multiobjective optimization technique. *Mech. Syst. Signal Process.* **2007**, *21*, 2295–2317. [CrossRef]

52. Huang, M.; Guo, W.; Zhu, H.; Li, L. Dynamic test and finite element model updating of bridge structures based on ambient vibration. *Front. Archit. Civ. Eng. China* **2008**, *2*, 139–144. [CrossRef]

53. Minshui, H.; Hongping, Z. Finite element model updating of bridge structures based on sensitivity analysis and optimization algorithm. *Wuhan Univ. J. Nat. Sci.* **2008**, *13*, 87–92. [CrossRef]

54. Bayraktar, A.; Altunisik, A.; Sevim, B.; Turker, T. Finite Element Model Updating of Komurhan Highway Bridge. *Tech. J. Turk Chamb Civ. Eng* **2009**, *20*, 4675–4700.

55. Schlune, H.; Plos, M.; Gylltoft, K. Improved bridge evaluation through finite element model updating using static and dynamic measurements. *Eng. Struct.* **2009**, *31*, 1477–1485. [CrossRef]

56. Yue, L.N.; Li, S. The Finite Element Model Updating of Long Span Cable-Stayed Bridge Based on Static and Dynamic Loading Test. *Appl. Mech. Mater.* **2014**, *644–650*, 5014–5018. [CrossRef]

57. Xiao, X.; Xu, Y.L.; Zhu, Q. Multiscale Modeling and Model Updating of a Cable-Stayed Bridge. II: Model Updating Using Modal Frequencies and Influence Lines. *J. Bridge Eng.* **2015**, *20*, 04014113. [CrossRef]

58. Zhong, R.; Zong, Z.; Niu, J.; Liu, Q.; Zheng, P. A multiscale finite element model validation method of composite cable-stayed bridge based on Probability Box theory. *J. Sound Vib.* **2016**, *370*, 111–131. [CrossRef]

59. Omenzetter, P.; Brownjohn, J.M.W.; Moyo, P. Identification of unusual events in multi-channel bridge monitoring data. *Mech. Syst. Signal Process.* **2004**, *18*, 409–430. [CrossRef]

60. Sohn, H.; Farrar, C.R.; Hemez, F.; Stinemates, D.W.; Nedler, B.; Czarnecki, J. *A Review of Structural Health Monitoring Literature 1996–2001*; Los Alamos National Laboratory: Los Alamos, NM, USA, 2004; ISBN LA-13976-MS.

61. Wenzel, H. *Health Monitoring of Bridges*; John Wiley & Sons: Hoboken, NJ, USA, 2008; Volume 20, p. 652. ISBN 0-470-74018-3.

62. Cross, E.J.; Koo, K.Y.; Brownjohn, J.M.W.; Worden, K. Long-term monitoring and data analysis of the Tamar Bridge. *Mech. Syst. Signal Process.* **2013**, *35*, 16–34. [CrossRef]

63. Farrar, C.R.; Doebling, S.W.; Nix, D.A. Vibration–based structural damage identification. *Philos. Trans. R. Soc. Lond. Ser. A Math. Phys. Eng. Sci.* **2001**, *359*, 131–149. [CrossRef]

64. Jaishi, B.; Ren, W.-X. Damage detection by finite element model updating using modal flexibility residual. *J. Sound Vib.* **2006**, *290*, 369–387. [CrossRef]

65. Banaś, A.; Wilde, K. Vibration diagnostics of footbridge with use of rotation sensor. *Appl. Comput. Sci.* **2014**, *10*, 38–49.

66. Jiménez-Alonso, J.F.; Pérez-Aracil, J.; Hernández Díaz, A.M.; Sáez, A. Effect of Vinyl Flooring on the Modal Properties of a Steel Footbridge. *Appl. Sci.* **2019**, *9*, 1374. [CrossRef]

67. Venuti, F.; Bruno, L. Crowd-structure interaction in lively footbridges under synchronous lateral excitation: A literature review. *Phys. Life Rev.* **2009**, *6*, 176–206. [CrossRef]

68. Li, Q.; Fan, J.; Nie, J.; Li, Q.; Chen, Y. Crowd-induced random vibration of footbridge and vibration control using multiple tuned mass dampers. *J. Sound Vib.* **2010**, *329*, 4068–4092. [CrossRef]

69. Jones, C.A.; Reynolds, P.; Pavic, A. Vibration serviceability of stadia structures subjected to dynamic crowd loads: A literature review. *J. Sound Vib.* **2011**, *330*, 1531–1566. [CrossRef]

70. Gao, Y.; Wang, J.; Liu, M. The Vertical Dynamic Properties of Flexible Footbridges under Bipedal Crowd Induced Excitation. *Appl. Sci.* **2017**, *7*, 677. [CrossRef]

71. Chen, Z.; Chen, S.; Ye, X.; Zhou, Y. A Study on a Mechanism of Lateral Pedestrian-Footbridge Interaction. *Appl. Sci.* **2019**, *9*, 5257. [CrossRef]

72. Pańtak, M. Ground Reaction Forces Generated by Runners—Harmonic Analyses and Modeling. *Appl. Sci.* **2020**, *10*, 1575. [CrossRef]

73. Racic, V.; Pavic, A.; Brownjohn, J.M.W. Experimental identification and analytical modeling of human walking forces: Literature review. *J. Sound Vib.* **2009**, *326*, 1–49. [CrossRef]

74. Alves, F. *Low-Cost Vibration Sensors: Tendencies and Applications in Condition Monitoring of Machines and Structures*; Instituto Superior de Engenharia de Lisboa: Lisboa, Portugal, 2015.

75. Van Emmerik, T.; Steele-Dunne, S.; Hut, R.; Gentine, P.; Guerin, M.; Oliveira, R.S.; Wagner, J.; Selker, J.; Van de Giesen, N. Measuring Tree Properties and Responses Using Low-Cost Accelerometers. *Sensors* **2017**, *17*, 1098. [CrossRef]

76. Jaroszewicz, L.R.; Kurzych, A.; Krajewski, Z.; Marć, P.; Kowalski, J.K.; Bobra, P.; Zembaty, Z.; Sakowicz, B.; Jankowski, R. Review of the Usefulness of Various Rotational Seismometers with Laboratory Results of Fibre-Optic Ones Tested for Engineering Applications. *Sensors* **2016**, *16*, 2161. [CrossRef] [PubMed]

77. Rossing, T.; Fletcher, N.H. *Principles of Vibration and Sound*, 2nd ed.; Springer: New York, NY, USA, 2004; ISBN 978-0-387-40556-8.

78. De Silva, C.W. *Vibration and Shock Handbook*; Taylor & Francis Inc.: Bosa Roca, USA, 2005.

79. Clough, R.W.; Penzien, J. *Dynamics of Structures*; Pearson Education: Upper Saddle River, NJ, USA, 1975.

80. Bianchi, G.; Sorrentino, R. *Electronic Filter Simulation & Design*; McGraw-Hill Education: New York, NY, USA, 2007; ISBN 978-0-07-149467-0.

81. Allemang, R.J.; Brown, D.L. A correlation coefficient for modal vector analysis. In Proceedings of the First International Modal Analysis Conference, Orlando, FL, USA, 8–10 November 1982; pp. 110–116.

82. Factors affecting perception thresholds of vertical whole-body vibration in recumbent subjects: Gender and age of subjects, and vibration duration. *J. Sound Vib.* **2011**, *330*, 1810–1828. [CrossRef]

83. Drygala, I.J.; Dulinska, J.M.; Polak, M.A. Seismic Assessment of Footbridges under Spatial Variation of Earthquake Ground Motion (SVEGM): Experimental Testing and Finite Element Analyses. *Sensors* **2020**, *20*, 1227. [CrossRef]